THE JOURNAL OF PHYSICAL CHEMISTRY B

pubs.acs.org/JPCB Article

How Alcoholic Disinfectants Affect Coronavirus Model Membranes: Membrane Fluidity, Permeability, and Disintegration

Hossein Eslami,* Shubhadip Das, Tianhang Zhou, and Florian Müller-Plathe

Cite This: *J. Phys. Chem. B* 2020, 124, 10374–10385 Read Online

ACCESS | Metrics & More | Article Recommendations | Supporting Information

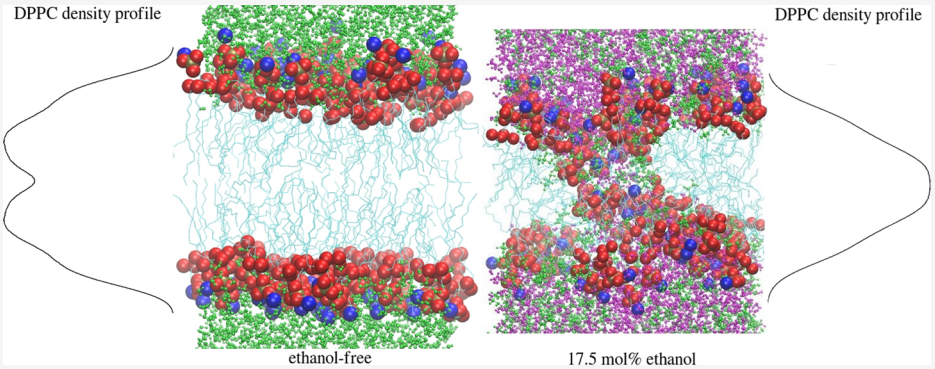

ABSTRACT: Atomistic molecular dynamics simulations have been carried out with a view to investigating the stability of the SARS-CoV-2 exterior membrane with respect to two common disinfectants, namely, aqueous solutions of ethanol and *n*-propanol. We used dipalmitoylphosphatidylcholine (DPPC) as a model membrane material and did simulations on both gel and liquid crystalline phases of membrane surrounded by aqueous solutions of varying alcohol concentrations (up to 17.5 mol %). While a moderate effect of alcohol on the gel phase of membrane is observed, its liquid crystalline phase is shown to be influenced dramatically by either alcohol. Our results show that aqueous solutions of only 5 and 10 mol % alcohol already have significant weakening effects on the membrane. The effects of *n*-propanol are always stronger than those of ethanol. The membrane changes its structure, when exposed to disinfectant solutions; uptake of alcohol causes it to swell laterally but to shrink vertically. At the same time, the orientational order of lipid tails decreases significantly. Metadynamics and grand-canonical ensemble simulations were done to calculate the free-energy profiles for permeation of alcohol and alcohol/water solubility in the DPPC. We found that the free-energy barrier to permeation of the DPPC liquid crystalline phase by all permeants is significantly lowered by alcohol uptake. At a disinfectant concentration of 10 mol %, it becomes insignificant enough to allow almost free passage of the disinfectant to the inside of the virus to cause damage there. It should be noted that the disinfectant also causes the barrier for water permeation to drop. Furthermore, the shrinking of the membrane thickness shortens the gap needed to be crossed by penetrants from outside the virus into its core. The lateral swelling also increases the average distance between head groups, which is a secondary barrier to membrane penetration, and hence further increases the penetration by disinfectants. At alcohol concentrations in the disinfectant solution above 15 mol %, we reliably observe disintegration of the DPPC membrane in its liquid crystalline phase.

INTRODUCTION

Alcohols are known to have immediate impact against many different enveloped viruses, including the new infectious coronavirus (2019-nCoV), also known as SARS-CoV-2 and HcoV-19.[1] Concentrated ethanol and propanol solutions in water (60−70 wt %), known as disinfectants, can inactivate coronavirus infectivity within seconds.[1] Experimental observations reveal that alcohols increase the area per lipid molecule, reduce the bilayer thickness, and hence destabilize the membranes.[2,3] Molecular simulations also confirm that small amphiphilic molecules dissolve in the membrane lipid and cause structural changes, including modification of bilayer packing and influencing the lipid acyl chain order, the phase transition temperature, and corresponding self-assembling properties of bilayer vesicles.[4,5] Such alcohol-induced structural changes in bilayers alter membrane function, influence the shape and stability of the cells and liposomes, and affect the conformational state of transmembrane proteins and their functions. As the membrane acts as a barrier to the passage of small molecules through it, the role and function of alcohols in

Received: September 11, 2020
Revised: October 28, 2020
Published: November 11, 2020

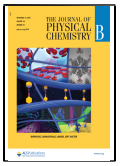

https://dx.doi.org/10.1021/acs.jpcb.0c08296
J. Phys. Chem. B 2020, 124, 10374−10385

the structural changes in lipid membranes depend on the permeability of the membrane to alcohols. The membrane is also responsible for mechanically anchoring the spike proteins, used by virus for fusion to the host cell membranes for facilitating viral entry into the host cell.[6] Alcohol-induced softening of the membrane may cause the loss of infectious proteins, even prior to the membrane rupture.

The composition of SARS-CoV-2 is not known; however, it is known that its viral envelope is derived from the host cell's membrane[6] and its genome encodes four structural proteins, sixteen nonstructural proteins, and nine accessory proteins, many of which are required to form a complete infectious viron.[7] Although the structure of the lipid membrane of SARS-CoV-2 is not known, there is experimental evidence for structural similarities between SARS-CoV and HIV.[8] For example, it is known that the membranotropic regions of both SARS-CoV envelope spike glycoprotein and the membrane fusion protein of HIV are located in a similar place of the protein sequence. In this respect, the HIV protease inhibitors are being considered as therapeutics for COVID-19 in recent clinical trials.[9] Experimental observations indicate that SARS and HIV proteins permeabilize the phospholipid membranes[10] and influence the membrane curvature and its size.[11] Also, the coronavirus envelope protein forms ion channels with membrane lipids; the activity of ion channels depends on whether they are formed in neutral or charged lipid bilayers.[12]

The large size of coronavirus (the diameter of SARS-CoV-2 is reported to be ≈0.1 μm)[13] together with the complex structure of its viral membrane, as explained, prevents us to model and simulate it as a whole. However, it seems logical to focus on a smaller membrane fragment. As the most important lipid components of living organisms are phosphatidylcholines (PCs), here we concentrate on a model membrane, namely, pure dipalmitoylphosphatidylcholine (DPPC), which serves as a useful model for understanding the physical properties of biological membranes. There is evidence allowing us to reasonably justify simulating DPPC as a model of coronavirus membrane. For example, it is known that coronavirus particles are replicated and assembled in the endoplasmic reticulum−Golgi intermediate compartment (ERGIC), and the particles budded into the ERGIC are trafficked for release by exocytosis.[14,15] Therefore, the coronavirus membrane is likely to be composed of PCs, as the main components of the ERGIC. Moreover, we know that the lung is the primary organ affected by coronavirus and DPPC is the most abundant constituent of lung surfactants.[16]

In addition, based on experimental reports on the permeabilization of phospholipid membranes in the presence of SARS peptides[10] and reduction of the gel-to-liquid crystalline phase transition temperature of the membrane[17] in the presence of the HIV virus protein, we argue that the liquid crystalline phase of the DPPC is its most biologically relevant state. Another line of evidence is that a pulmonary surfactant, from which possibly the virus takes its membrane, is composed of DPPC (as the main component) mixed with PMPC, PPPC, and POPC; mixtures of the latter three membranes with DPPC have lower gel-to-liquid crystalline phase transition temperatures than pure DPPC.[18,19] These observations imply that the fluid (liquid crystalline) phase of bilayer is the most physically relevant phase to the inactivation of SARS-CoV-2 infectivity by alcohol. Therefore, as a first step in the elucidation of the mechanism of action of disinfectant molecules on the viral membrane, we have performed simulations on DPPC at 323 K (corresponding to the liquid crystalline phase of the membrane)[20] immersed in water−alcohol solutions of various concentrations. As the disinfectants are used at room temperature, we have also done simulations at lower temperatures, 298 K (where the DPPC exists in the gel phase)[20] to study influence of disinfectants on the membrane at room temperature and to examine the temperature dependence of the stability of the SARS-CoV-2.[21]

The term permeability refers to the overall mass transport of penetrant molecules (alcohols as well as others) across the membrane. This process involves the solubility of water-borne alcohol molecules in the lipid phase followed by their diffusion through the membrane. Due to its significance, there exist numerous studies on alcohol interaction with lipid bilayers in the literature. Among these studies, molecular simulations have provided a useful tool to elucidate the mechanism of permeation of small molecules in membranes.[22−27] For a comprehensive list of simulation studies focusing on lipid bilayers, the reader is referred to a recent review by Venable et al.[28] Although simulations of this type have been successful in providing a molecular-level basis for alcohol penetration through membranes, the majority of them are limited to low concentrations of alcohol (in the aqueous phase). In the majority of simulation studies, the aim has been to calculate the free-energy barrier underlying the translocation of penetrant alcohol across the lipid bilayer and to examine the mechanism of penetrant permeation (at infinite dilution) across the membrane. Typically, for calculating the free-energy profile, a single alcohol molecule was transferred from the aqueous phase (infinite dilution) into the lipid phase. In contrast, there are only a few reports[20,29−31] on the concentration dependence of alcohol penetration through the membrane and the partition coefficient of alcohol between aqueous and lipid phases in concentrated alcohol solutions, where ethanol-induced "damage" to the bilayer structure becomes an issue of importance. High alcohol concentrations (60−70 wt %)[1] are, however, the common concentration range in alcohol-based disinfectants, which are able to terminally destabilize membranes.

Here, we systematically examine alcohol (ethanol as well as *n*-propanol) solubility in DPPC and study the dependence of the partition coefficient on the alcohol concentration in the aqueous phase. The range of concentrations examined varies from low concentrations at which alcohol only partitions between the two phases to high concentrations at which alcohol disrupts the membrane. This study provides insight not only into the mechanism of disinfectant influence on the membrane functionality but also on its effect on lipid properties in the membrane. In addition to disinfection, modulation of functions of biological membranes by alcohols has numerous aspects in applications such as drug delivery, anesthesia, and cryopreservation; for example, high concentrations of ethanol are used, as penetration enhancers, in transdermal drug delivery.[32]

SIMULATIONS

We performed atomistic molecular dynamics (MD) simulations to investigate the interaction between ethanol and *n*-propanol with DPPC as a model lipid bilayer membrane. We have done two sets of simulations; one set at 323 K (above the gel-to-liquid crystalline phase transition temperature of DPPC, 315 K)[20] and another at 298 K (where DPPC exists in the gel phase). Simulations were done for a number of systems in

https://dx.doi.org/10.1021/acs.jpcb.0c08296
J. Phys. Chem. B 2020, 124, 10374−10385

which the concentration of ethanol varied systematically from 0 to 17.5 mol % and that of *n*-propanol varied from 0 to 15.0 mol %. Unless mentioned otherwise, the term concentration always refers to the concentration of alcohol in the water phase in mole percent, based on the total number of water molecules in the system, i.e., outside the lipid bilayer. This corresponds to 35.2 and 37.0 wt % for ethanol and *n*-propanol, respectively. Reference systems consisting of a bilayer of total 64 DPPC lipid molecules surrounded with water (6400 molecules at 298 K and 3000 molecules at 323 K) were simulated. In both systems, the number of water molecules per lipid was in the range reported experimentally.[33] The lipid molecules and water were placed into a rectangular simulation box, where the bilayer extends in the *xy* plane and the *z* direction defines the bilayer normal (the area per lipid in the initial simulation box at 323 K was 0.63 nm^2, and the membrane thickness was 4.1 nm). In the alcohol-containing systems, the numbers of water and lipid molecules in the system were the same, but alcohol molecules were added to the aqueous phase to reach the desired concentration of alcohol in water. We have simulated 12 alcohol-containing systems in which the concentration of either ethanol or *n*-propanol varies from ≈5 mol % to ≈17.5 mol %. The alcohol mol % is defined based on the number of alcohol, $n_{alcohol}$, and water, n_{water}, molecules (disregarding the lipids) in the system, i.e., mol $\%_{alcohol} = 100\ n_{alcohol}/(n_{alcohol} + n_{water})$. The details of systems simulated in this work are tabulated in Table 1. We did not simulate higher alcohol concentration systems because they invariably cause rupture of the membrane (at 323 K, at concentration higher than 15 mol % alcohol).

Lipid molecules were described by the all-atom CHARMM36 potential energy function.[34] All simulations were done using the software YASP.[35] The temperature and pressure were kept fixed using a Berendsen thermostat and Berendsen barostat[36] (the time constants for temperature and pressure couplings were 0.2 and 4.0 ps, respectively). The simulation box size in the lateral and normal directions was allowed to change independently to keep the lateral and normal components of pressure fixed at 101.3 kPa. The Berendsen thermostat and barostat are known to suppress fluctuations; however, perturbations in the simulation box due to particle insertions/deletions during the course of the grand canonical ensemble (GCE) simulations include fluctuations in the system. The equations of motion were solved using the leapfrog integration scheme[37] with a time step of 2 fs. The cutoff for nonbonded interactions was 1.0 nm, treating electrostatic interactions by the reaction-field approximation.

Alcohol solubility calculations in the liquid crystalline phase of DPPC were done in the GCE (see below). At low temperatures (298 K) where the DPPC exists in the gel phase, due to tight packing of lipid molecules, the alcohol solubility is very low. In this case, we did long-time (up to 750 ns) *NPT* ensemble simulations, on DPPC in contact with alcohol solutions and monitored direct partitioning of alcohol between aqueous and lipid phases.

It is worth mentioning that while the size of the DPPC bilayer simulated in this work locates within the range normally simulated in the literature, recent simulation reports focusing on the artifacts of periodic boundary conditions in small systems reveal that free energies for translocation of charged cationic peptides across the membranes[38] and for transmembrane pore formation[39] depend on the system size. Based on these reports, our calculated Gibbs free energies for translocation of penetrants across the lipid bilayer, and hence, the alcohol solubilities in the DPPC might depend on the system size.

Table 1. Description of Systems Simulated in This Work[a]

system[b]	composition[c] (mole fraction of alcohol)	average surface area (nm^2)	membrane thickness (nm)	number of alcohol molecules
1	0	0.64	3.86	0
2	0.052 (12.3 wt %) ethanol	0.82	3.18	165
3	0.104 (22.9 wt %) ethanol	0.94	2.85	348
4	0.150 (31.1 wt %) ethanol			530
5	0.053 (15.7 wt %) *n*-propanol	0.83	3.15	168
6	0.103 (27.7 wt %) *n*-propanol	0.97	2.82	345
7	0.150 (37.0 wt %) *n*-propanol			530
8	0.175 (35.2 wt %) ethanol			1360
9	0	0.496	4.35	0
10	0.050 (11.8 wt %) ethanol	0.486	4.38	340
11	0.096 (21.3 wt %) ethanol	0.490	4.37	680
12	0.175 (35.2 wt %) ethanol	0.495	4.38	1360

[a]The mole fraction of alcohol is defined based on the number of alcohol and water molecules in the system (lipid-free basis). [b]Simulations for systems 1−8 and 9−12 are done at 323 and 298 K, respectively. For alcohol-containing systems, higher temperature simulations (except for system 8) are done in the grand canonical ensemble for solubility calculations. For systems 8−12, simulations are done in the *NPT* ensemble. The numbers of water molecules in systems 1−7 and in systems 8−12 are 3000 and 6400, respectively. [c]The numbers in parenthesis are the weight percents of alcohol.

METHODS

The solubilities of ethanol, propanol, and water in DPPC at 323 K have been calculated employing our GCE MD simulation scheme.[40] Previously, we have applied it to calculate the solubilities of small penetrant molecules in polymers.[41−43] The details of the method are explained in Ref 40. Here, we restrict ourselves to a brief explanation. In the GCE simulation formalism, the system is open, i.e., the number of lipid molecules in the system is kept constant, but water, ethanol, and *n*-propanol molecules are exchanged between the system and an ideal gas reservoir. The potential energy of interaction of the molecules to be exchanged between the system and reservoir (fractional molecules) with the rest of the system is scaled by a coupling parameter, λ, ranging between zero and one. At the two extremes, where λ goes to zero or to 1, the fractional molecule is decoupled from or fully coupled to the system, respectively. The exchange of molecules between the system and the material reservoir is ruled by the following equation:

$$W\frac{d^2\lambda}{dt^2} = -\sum_{i=1}^{N}\frac{\Delta U_{if}}{\Delta\lambda} + \mu - k_B T \ln\left[\left(\frac{2\pi m k_B T}{h^2}\right)^{3/2}\frac{N}{V}\right] \quad (1)$$

where W is the mass associated with the additional coordinate λ, t is the time, U_{if} is the potential energy of interaction

https://dx.doi.org/10.1021/acs.jpcb.0c08296
J. Phys. Chem. B 2020, 124, 10374−10385

between the fractional and host particles, N is the total number of particles in the system, μ is the target chemical potential, k_B is the Boltzmann constant, T is the temperature, h is Planck's constant, and V is the volume. In fact, the sum of the last two terms on the right hand side of eq 1 is the excess chemical potential, μ^{ex}, defined as the difference between the chemical potential and the chemical potential of the ideal gas at the same temperature and density.

To remove overlaps between the inserted fractional molecules and the host particles, we have employed a soft-core potential, proposed by Rahbari et al.,[44]

$$U_{if} = 4\varepsilon_{if}\left[\frac{1}{\left(\frac{1}{2}(1-\lambda)+\left(\frac{r_{if}}{\sigma_{if}}\right)^6\right)^2} - \frac{1}{\frac{1}{2}(1-\lambda)+\left(\frac{r_{if}}{\sigma_{if}}\right)^6}\right] \quad (2)$$

where ε is the potential well depth and σ is the position at which $U = 0$, r is the distance, and subscripts i and f stand for ordinary (host) and fractional particles, respectively. This potential allows for overlap between the fractional molecule and the host molecules. Meanwhile, as the fractional molecule grows ($\lambda \rightarrow 1$), the potential converges to the conventional Lennard-Jones (12−6) potential. Solving eq 1, penetrant molecules are added to and/or removed from the system until achieving equilibrium, defined as a stage at which the number of penetrant molecules fluctuates around an average value, consistent with the fixed values of temperature, volume, and excess chemical potential.

To calculate the local densities of penetrants inside the bilayer and in the surrounding aqueous solution, we first perform a GCE simulation of the water−alcohol mixtures at prespecified concentrations. The excess chemical potentials of water and alcohol in such a solution are calculated by dynamically inserting/removing molecules into/from the simulation box during the course of GCE simulation. Then, we perform GCE simulation of the bilayer systems in which the bilayer is surrounded by an aqueous solution of the alcohol. First, we insert a few water and alcohol molecules (below their solubility) into the bilayer. The simulation box is divided along the z direction (membrane normal) into a number of slabs, and the excess chemical potential in each slab is set according to the predetermined excess chemical potentials of alcohol in the aqueous phase and the local density (see eq 1). During the course of GCE simulation, water and alcohol molecules are exchanged between each slab and the material reservoir, till the density in each slab fluctuates around a constant value.

RESULTS

Validation of the DPPC Model. To validate the lipid bilayer model simulated in this work, we have calculated the area per phospholipid head group of a DPPC bilayer in pure water (no alcohol). This is one of the most important quantities, which controls other structural and dynamical properties of the bilayer such as its thickness, ordering, and the lateral diffusion of lipids. Our calculated area per lipid head group is 0.645 nm^2 at 323 K, which is in very good agreement with previous simulation results (0.655 nm^2 by Patra et al.,[45] 0.63 nm^2 by Cordomi et al.[46] and by Bemporad et al.,[47] and 0.66 nm^2 by Bassolino-Klimas et al.[48]) and with the experiment[49] (0.69 nm^2) all at 323 K. In addition, our calculated surface area per lipid at 298 K (0.496 nm^2) also agrees well with experimental data[50] (0.487 nm^2) and former simulation results by Schubert et al.[51] at 300 K (0.50 nm^2).

Construction of the Free-Energy Profile. At equilibrium, the chemical potential of all solutes is equal in all phases. Therefore, partitioning the simulation box along the z direction (membrane normal) into a number of slabs of specified thickness, the solute i has the same chemical potential in all slabs along the z direction. The local *excess* chemical potentials along the z direction are expressed in terms of the local densities as

$$\mu_i^{ex}(z) - k_B T \ln(\rho_i(z)) = \text{constant} \quad (3)$$

where $\rho(z)$ is the local number density. Adopting the aqueous phase surrounding the membrane as the reference state, one can write

$$\Delta G(z) = \mu_i^{ex}(z) - \mu_i^{ex}(\text{aqueous}) = -k_B T \ln\left(\frac{\rho_i(z)}{\rho_i(\text{aqueous})}\right) \quad (4)$$

where $\Delta G(z)$ stands for the transfer (molar) free energy from the reference state, aqueous phase, to the position z, also called the potential of mean force along the z coordinate.

As a control system, we have calculated free-energy profiles for transfer of water, ethanol, and propanol in a DPPC bilayer immersed in pure water, i.e., in the infinite-dilution limit. Performing successive insertions/deletions of water molecules in the aqueous phase, we have calculated $\mu^{ex}_{water.}$ Our calculated value (−27.5 kJ/mol) at 298 K is in very good agreement with reported values in the literature (−26 kJ/mol at 300 K).[52−54] Our calculated excess chemical potentials for ethanol and *n*-propanol in water at infinite dilution (hydration free energies) are −17.4 and −16.8 kJ/mol, which are close to former reported results for the same model (−17 for ethanol at 300 K)[55] and are in agreement with the experiment (−21.1 and −20.4 kJ/mol, respectively, at 300 K).[56] Note that in calculation of excess chemical potentials, the constant factor $k_B T \ln\left[\left(\frac{2\pi m k_B T}{h^2}\right)^{3/2}\right]$ in eq 1 is set to zero for the sake of simplicity.

We have done the same procedure to calculate $\mu^{ex}_{water}(z)$ in 0.5 nm thick slabs throughout the simulation box. During the course of the GCE simulation, the target $\mu^{ex}_{water}(z)$ is set (depending on the local density) according to eq 1, and simulations are done until the local density only fluctuates around an average value. The GCE simulation method provides quantitatively accurate results over the regions of the simulation box, where the local (equilibrium) density is sufficiently high to produce reliable statistics of the average local density during frequent insertions/deletions (normally a few molecules in each slab are sufficient for this purpose).

We noticed that at 298 K (gel phase of DPPC), the tight packing of lipid molecules does not allow noticeable alcohol/water solubility in the bilayer. Due to poor efficiency of the insertions in the GCE simulation in the gel phase of DPPC, we have calculated free-energy profiles for water and alcohol (at infinite dilution) employing an advanced sampling procedure, metadynamics.[57] In this case, we have employed our recently improved version of metadynamics, which imposes adaptive potentials, tuned on the fly, on the reaction coordinate (here: the center-of-mass z coordinate of the solute).[58,59] For all

https://dx.doi.org/10.1021/acs.jpcb.0c08296
J. Phys. Chem. B 2020, 124, 10374−10385

alcohol-containing systems at 298 K (see Table 1), simulations were done in the *NPT* ensemble, for long times (up to 750 ns) to examine direct partitioning of alcohol between the aqueous and the lipid phases. Also for system 1 (at 323 K), due to the low solubility of water in DPPC, the free-energy profile is calculated using metadynamics. For more concentrated alcohol solutions (≈5 and ≈10 mol %), the density of alcohol is high enough even in the center of the bilayer to provide reliable statistics in the GCE simulations. In this case, we do not need to resort to advanced sampling techniques to calculate the free-energy profile. Performing successive insertions/deletions of penetrant molecules into/from different regions of the simulation box until achieving a constant density in rectangular slabs (extending in the *xy* plane, i.e., parallel to the membrane), we have calculated equilibrium number density profiles, corresponding to constant and uniform chemical potentials.

In Figure 1, we have shown the free-energy profile across the DPPC bilayer for water and that for ethanol and *n*-propanol, at

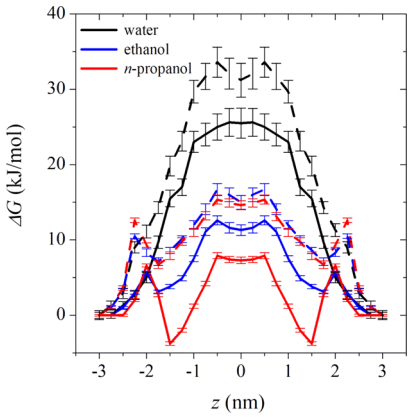

Figure 1. Free-energy profiles for translocation of water, ethanol, and *n*-propanol across the DPPC lipid bilayer immersed in pure water (infinite-dilution limit). The full and dashed curves represent free-energy profiles at 323 and 298 K, respectively. The position $z = 0$ corresponds to the center (hydrocarbon core) of the bilayer. The headgroups are at ≈ ± 2.0 nm and ≈ ± 2.2 nm for DPPC at 323 and 298 K, respectively. The chemical potential inside the aqueous phase is taken as zero.

infinite dilution: by moving one of the many water molecules or the single alcohol molecule in the z direction, while the aqueous phase contains only water. In this case, the low concentration of species in the bilayer necessitates the use of metadynamics for calculating the free-energy profiles. Because of the symmetry of the two leaflets of the membrane, the free-energy profiles were symmetrized.

For the sake of comparison, we have also shown the density profiles for the center of mass of the phosphate head groups of the bilayer in Figure 2. The head groups of the alcohol-free bilayer show two well-resolved peaks at ≈2.0 nm (298 K) and ≈2.0 nm (323 K) from the center of the bilayer.

The structural inhomogeneity of the membrane causes solubility inhomogeneity of penetrants across the membranes; water does not well dissolve in the polar head group region of the membrane but even less inside the lipid phase. The hydrophilic head group of the bilayer produces barriers at $z \approx$ 2 nm from the bilayer center (at 298 and 323 K, respectively), corresponding to the positions of phosphate peaks in Figure 2, to the passage of the hydrophobic penetrants. This barrier depends on the temperature, hydrophilicity, and the size of

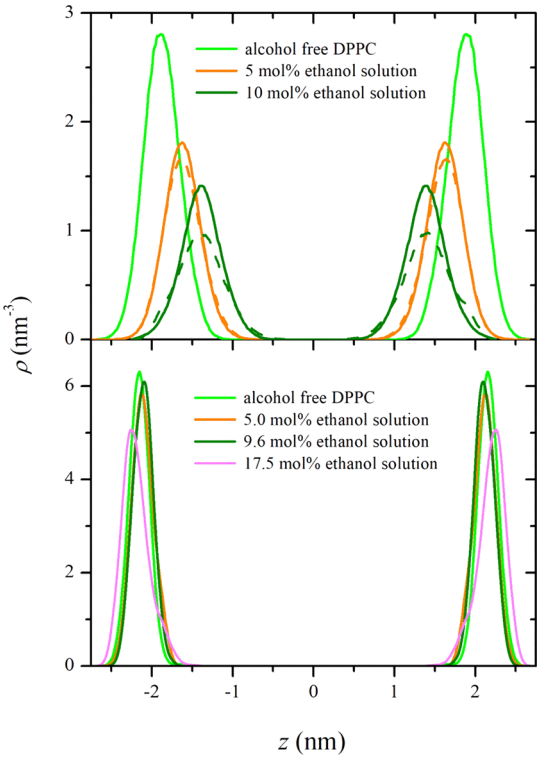

Figure 2. Number density profiles for the centers of mass of phosphate head groups of DPPC at 323 K (top panel) and 298 K (bottom panel). The compositions of the systems are shown in the figure's legend. In the top panel, the dashed curves indicate the profiles for phosphate head groups in *n*-propanol solutions; mole fractions of ethanol (*n*-propanol) in ≈5 mol % and ≈10 mol % solutions are 0.520 (0.530) and 0.104 (0.103), respectively.

penetrant molecules; it is higher for the bigger and more hydrophobic molecule (*n*-propanol). The smaller-size hydrophilic molecules, like water, more easily cross this barrier to dissolve in the hydrophilic domains of the membrane. Following the barrier due to the dense hydrophilic lipid head groups, the free-energy profile for ethanol and *n*-propanol passes through a local minimum (at $z \approx$ 1.7 nm from the bilayer center at 298 K and $z \approx$ 1.5 nm at 323 K) at the encounter of polar head groups and nonpolar hydrocarbon chains (see Figure 2 for comparison). In this region, alcohol preferentially dissolves in the head−tail interphase of the lipid. For all penetrants, the largest barrier height is observed very close to the center of the membrane ($z \approx 0$). Because of the existence of a larger free volume at the immediate membrane center ($z = 0$), the free energy is marginally more favorable than that in its close neighborhood. Reasonably, this barrier is higher for penetration of hydrophilic solutes and decreases with increasing the hydrophobicity of the solute. This implies that propanol more easily crosses the lipid tail group of the membrane than ethanol and water. The hydrophobic region of the membrane is more permeable to the passage of more hydrophobic molecules (*n*-propanol). Furthermore, the barrier height depends on the temperature. In agreement with former simulations,[44] much tighter packing of lipid molecules in the DPPC gel phase, compared to that for the liquid crystalline phase, is observed (see the density profile peaks in Figure 2). While addition of alcohol to the system reduces the order of the head groups at 323 K, it has no pronounced effect on the order of head groups in the gel phase. At 298 K, the profile for

https://dx.doi.org/10.1021/acs.jpcb.0c08296
J. Phys. Chem. B 2020, 124, 10374−10385

the centers of mass of phosphate head groups at 17.5 mol % ethanol shows wider distributions (compared to those for lower ethanol concentration), indicating that alcohol has a noticeable fluidizing effect on the bilayer at this concentration.

The tight packing of lipid molecules in the gel phase explains its low permeability to alcohol and water. In fact, the low solubility of ethanol and water in the gel phase of DPPC does not allow us to perform GCE simulations of the solubility. Therefore, all gel-phase simulations are done in the *NPT* ensemble (over a long time, up to 750 ns), letting alcohol/water molecules in the aqueous phase to find their natural pathway to the lipid phase of the bilayer.

We have also shown in Figures 3 and 4 the free-energy profiles for water, ethanol, and *n*-propanol for membranes

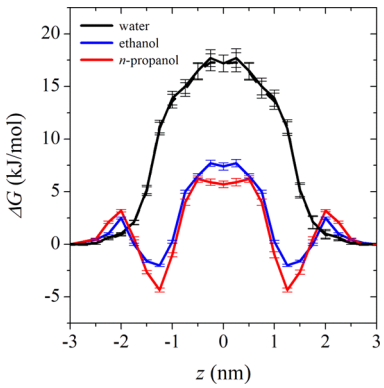

Figure 3. Free-energy profiles for translocation of water, ethanol, and *n*-propanol across a DPPC lipid bilayer surrounded by an aqueous phase containing 5.2 mol % ethanol and 5.3 mol % *n*-propanol at 323 K. The black full and dashed curves indicate free-energy profiles for water in ethanol and *n*-propanol solutions, respectively.

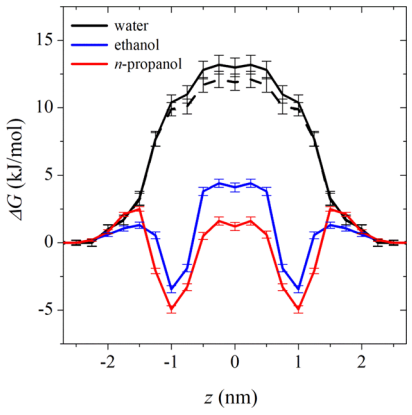

Figure 4. Free-energy profiles for translocation of water, ethanol, and *n*-propanol across a DPPC lipid bilayer surrounded by an aqueous phase containing 10.4 mol % ethanol and 10.3 mol % *n*-propanol at 323 K. The black full and dashed curves indicate free-energy profiles for water in ethanol and *n*-propanol solutions, respectively.

immersed in solutions in contact with ≈5 mol % and ≈10 mol % alcohol at 323 K. The barrier formed by the head groups decreases with the increasing alcohol content. This can be interpreted by the lateral expansion of the membrane in the presence of alcohol (see below). Furthermore, a close look at the density profile peaks for phosphate head groups in Figure 2 shows that in alcohol-containing systems, the head group peaks are wider but shift closer to the bilayer center (the positions of the maxima in ≈5 mol % and ≈10 mol % alcohol solutions are at 1.6 nm and ≈1.4 nm from the bilayer center). Widening of the head group distributions with the increasing alcohol content, simultaneous with a shrinking distance between them, suggests that alcohol disturbs the order of the lipid head groups and causes the bilayer thickness to decrease. Therefore, the defects introduced into the membrane, as a result of its lateral expansion, make the head-group region more permeable to small penetrant molecules, including water. The local minimum at the membrane hydrophilic−hydrophobic interphase decreases further with the increasing alcohol concentration. In other words, water and alcohol molecules have a higher tendency to accumulate in this interphase (compared to the alcohol-free systems) as a result of decrease in the density. Finally, also the highest barrier at the hydrophobic core of the membrane ($z \approx 0$) becomes more permeable to the passage of all penetrants with the increasing alcohol concentration. At higher alcohol concentrations (compared to the infinite dilution regime), the free energy cost for transfer of alcohol molecules into the bilayer is lower. Interestingly, addition of alcohol to the membrane also decreases the free-energy cost for transfer of water into the membrane. Both effects are more dominant at higher alcohol concentrations.

The largest barrier for water, ethanol, and *n*-propanol is nearly always found at the center of the membrane, i.e., in the hydrophobic core, where the tails of the two leaflets meet. Addition of alcohol universally reduces this barrier (see Figure 5). The largest barriers are seen for water, the lowest for *n*-

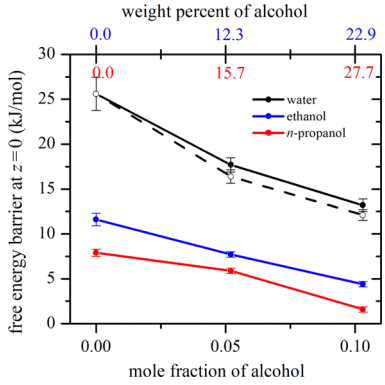

Figure 5. Free-energy barrier to permeation of the membrane as a function of external alcohol concentration at 323 K. The position z = 0 corresponds to the center (hydrocarbon core) of the bilayer. The black full and dashed curves indicate free-energy barriers for water permeation in the membrane, immersed in ethanol and *n*-propanol solutions, respectively. The weight percents of ethanol and *n*-propanol are shown on the top axis in blue and red, respectively.

propanol. For both alcohols, they become easily surmountable at a mole fraction of 0.1 where they are about ≈2 k_BT and ≈1 k_BT for ethanol and *n*-propanol, respectively. At this disinfectant concentration, we expect therefore easy penetration of the membrane by the disinfectant. For *n*-propanol, the energy barrier at the membrane core is lowered to such an extent at 10.0 mol % that it falls below the barrier in the head group region (2.5 kJ/mol, Figure 4), which is an exception.

Using the free-energy barriers as a zero-order estimate for the activation energy of a membrane-crossing event and using as an example the values for water at 0% alcohol (26.0 kJ/mol = 9.7 k_BT) and 10 mol % (13.0 kJ/mol = 4.8 k_BT), we can make a rough estimate that the permeation of water (and

https://dx.doi.org/10.1021/acs.jpcb.0c08296
J. Phys. Chem. B 2020, 124, 10374−10385

hence of other water-borne penetrants) will be accelerated by 2 orders of magnitude in the presence of alcohol. The function of the membrane as protecting the coronavirus from noxious chemicals is, thus, significantly reduced in the presence of even a small concentration of alcohol.

Partitioning of Alcohol between Aqueous and Lipid Phases. We have shown the number density profiles for alcohol and water (calculated at 323 K) in Figure 6. They are

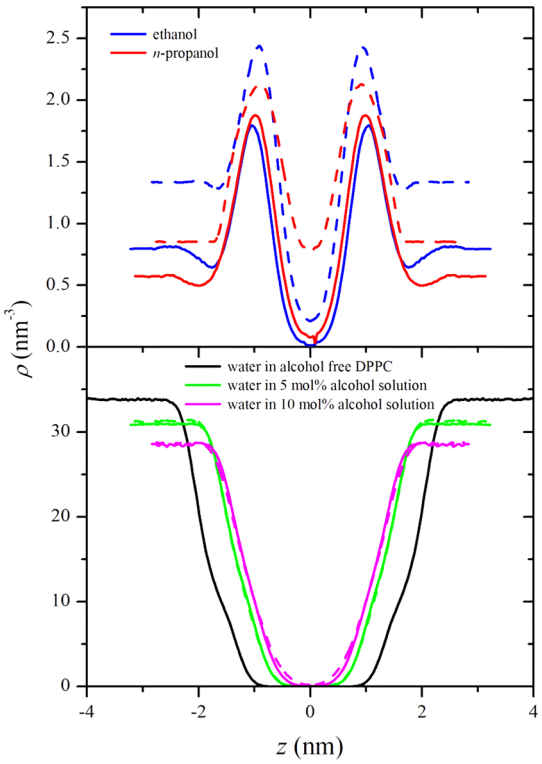

Figure 6. Top panel: Number density profiles for alcohol across the DPPC membrane immersed in solutions containing ≈5 mol % (full curves) and ≈10 mol % (dashed curves) ethanol and *n*-propanol at 323 K. Bottom panel: Number density profiles for water across the DPPC membrane immersed in alcohol solutions (the percentage of alcohol is shown in the figure) at 323 K. The full and dashed curves belong to ethanol and *n*-propanol solutions, respectively, and the black curve belongs to the alcohol-free solution. Mole fractions of ethanol (*n*-propanol) in ≈5 mol % and ≈10 mol % solutions are 0.520 (0.530) and 0.104(0.103), respectively.

essentially the Boltzmann inversions of the corresponding free-energy profiles (Figures 1, 3, 4). The (number) density profiles for alcohols show an increase of the alcohol concentration in the lipid phase of the bilayer with an increase of the alcohol concentration in the aqueous phase. The concentration of alcohol in the aqueous phase corresponds to distances larger than 2.5 and 2.0 nm from the center of the bilayer in solutions containing ≈5 mol % and ≈10 mol % alcohol, respectively). Near the head groups, there is a depletion of alcohol. This region is better resolved in less concentrated alcohol solution in which the head groups are better organized (denser). Increasing the alcohol concentration and hence decreasing the head group order remove this structure. The position of maxima in the alcohol density is just inside the head group regions indicating that alcohol dissolves preferentially in the head−tail interphase of the bilayer. This leads us to suspect that the solubility of the amphiphilic alcohol molecules is driven, on the one hand, by the interactions between the OH group of alcohol and the polar head groups of the membrane. On the other hand, the hydrophobic tail of alcohol dissolves in the hydrocarbon chain of the bilayer; this solvation mode is confirmed below. Very close to the center of the bilayer, the solubility of alcohol is low. Increasing the outside alcohol concentration, however, increases its solubility also at the center of the bilayer. We finally note that the concentration of water at the center of the bilayer is not increased by adding alcohol to the system. The lowering of the free-energy barrier for water (Figures 1, 3, 4) is not sufficient to cause an appreciable water concentration here. The influence of disinfectant alcohol on the membrane is primarily to enhance water permeation in the membrane but not to significantly increase the water concentration at the membrane center. Alcohol, however, has the effect of making the membrane thinner by about 1 nm. Accordingly, the gap of low water concentration inside the membrane becomes narrower.

Membrane Failure. Our GCE simulations show that the DPPC bilayer at 323 K undergoes disruption at 15 mol % ethanol or *n*-propanol. To determine whether failure is an artifact of the perturbation of the system by particle insertions and deletion or whether it is an alcohol-induced weakening effect, we also did a direct *NPT* ensemble simulation on DPPC immersed in a 17.5 mol % ethanol solution (system 8 in Table 1) at 323 K for a long time. We observed that in this direct simulation, ethanol introduces increasing disorder in the membrane, until at $t > 500$ ns, the membrane ruptures. This direct observation confirms the validity of our GCE simulations. Similar *NPT* simulations were done on DPPC surrounded by less concentrated ethanol solutions. No disruption was observed at lower ethanol concentrations (<15 mol %). We have shown snapshots of the simulation box, for a DPPC membrane surrounded by ethanol solutions of different concentrations, in Figure 7. Ethanol introduces a big hole in the DPPC membrane immersed in a 17.5 mol % ethanol solution. The same *NPT* simulations were done at 298 K; we have shown snapshots of the simulation box in Figure S1. At this lower temperature, where the membrane is in its gel phase, no sign of membrane disintegration was observed (up to 750 ns).

We have described the relevance of our solubility calculations and membrane rupture at 323 K (the liquid crystalline phase of DPPC) with inactivation of SARS-CoV-2 infectivity at room temperature, 298 K (where the disinfectants are used) in the introduction part.

Alcohol Solvation in the Membrane. To elucidate the mechanism of solvation of alcohol inside the membrane, we have shown in Figure 8 the density profiles for the hydroxyl-O and the terminal C atoms of the alcohol molecules as a function of z distance from bilayer head groups. For this analysis, the head group positions are not averaged, but we measure their z position and the distance in z of alcohol atoms from them, following the local corrugation of the membrane. For this purpose, we put an xy grid on the simulation box (spacing 0.5 nm × 0.5 nm) and averaged the density in each quadratic prism volume (situated at a given x and y) as a function of the z distance from the outermost head group atoms in this prism. The alcohol oxygens clearly are closer to the lipid head groups than the carbons. This indicates that favorable hydrophilic interactions between the hydroxyl groups and the lipid head group and van-der-Waals interactions between the alkane tails of the lipids and the alkyl rests of the

https://dx.doi.org/10.1021/acs.jpcb.0c08296
J. Phys. Chem. B 2020, 124, 10374−10385

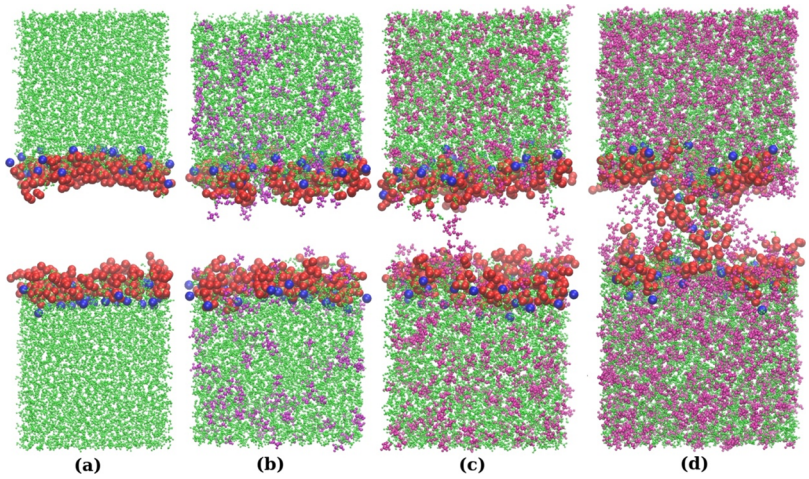

Figure 7. Snapshots of the simulation box for a DPPC membrane immersed in 0.0, 5.0, 9.6, and 17.5 mol % ethanol solutions (from a to d, respectively) at 323 K. The water and ethanol molecules are shown in green and purple, respectively, the blue and red spheres show P and O atoms of the lipid head group, respectively, and the lipid tails are not displayed for clarity. All snapshots are taken at t = 600 ns. At a concentration of 17.5 mol % ethanol (snapshot d), the DPPC bilayer undergoes disruption.

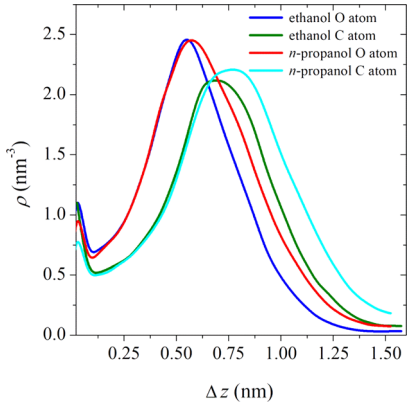

Figure 8. Number density profiles for alcohol O and terminal C atoms as a function of distance from the lipid head groups at 323 K. The full and dashed curves indicate profiles for ethanol and *n*-propanol, respectively.

alcohols lead to alcohol dissolving in the head−tail interphase of the membrane. Expectedly, the terminal C atom of *n*-propanol is located at farther distances from the membrane head group than that of ethanol.

We have also shown the density profiles for water and ethanol penetration in the DPPC bilayer immersed in pure water and in water−ethanol mixtures (up to 17.5 mol %) at 298 K in Figure 9. The results show that at higher ethanol concentrations, the membrane becomes more permeable to alcohol. Also in this case, we see alcohol-induced water solubility in the membrane. Of course, compared to the liquid crystalline phase of the membrane, both effects are less pronounced in the gel phase.

Effect of Ethanol on the Structure of the Lipid Bilayer. We have shown the surface area per lipid head group for DPPC surrounded by water−alcohol solutions in Table 1. The results show that while the gel phase of membrane is not considerably affected by the alcohol, both alcohols cause a dramatic increase of the surface area per lipid head group in the liquid crystalline phase of the membrane. In the liquid crystalline phase, both alcohols increase the surface area by nearly the same extent; *n*-propanol is only slightly more

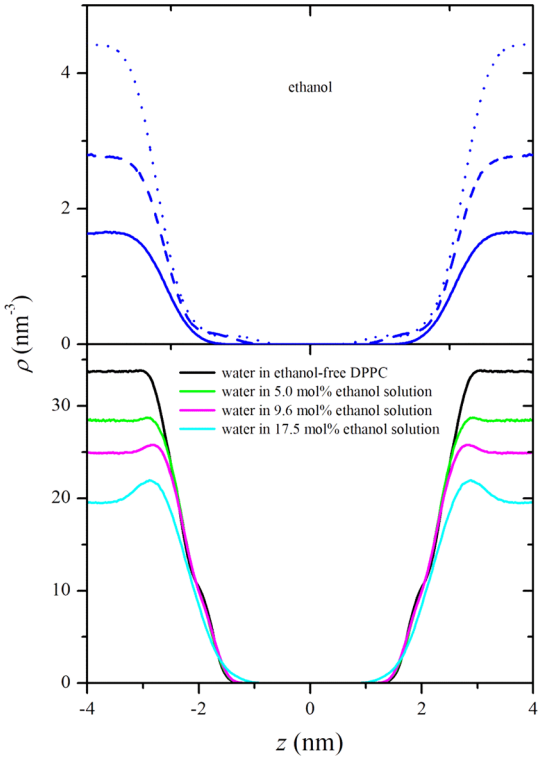

Figure 9. Number density profiles for ethanol (top panel) and water (bottom panel) in 5.0 mol % (full curves), 9.6 mol % (dashed curves), and 17.5 mol % (dotted curves) ethanol solutions at 298 K. The black curve shows the number density of water for the ethanol-free solution.

effective in this respect. At the same time, the membrane thickness is decreasing considerably as alcohol is taken up.

Both observations imply that alcohol has a disordering effect on the membrane. We have quantified the lipid-chain order in the presence and absence of alcohol in terms of a dimensionless order parameter, defined as

$$|S| = \frac{3}{2}\langle(\boldsymbol{u}_{CH}\cdot\boldsymbol{n})^2\rangle - \frac{1}{2} \quad (5)$$

https://dx.doi.org/10.1021/acs.jpcb.0c08296
J. Phys. Chem. B 2020, 124, 10374−10385

Because in experiment, the order in lipid chains is determined by means of deuterium nuclear magnetic resonance spectroscopy, it is also known as the deuterium order parameter. In eq 5, the unit vectors $\boldsymbol{u}_{CH}$ and $\boldsymbol{n}$ are along a C−H bond (C−D bond of the deuterated sample in experiment) and the bilayer normal, respectively. A value of $S = 1$ would indicate parallel alignment, a value $S = 0$ complete disorder. We have calculated the order parameter for all C−H bonds along the alkyl chains and shown it as a function of position in the chain (Figure 9). The results in Figure 10 show

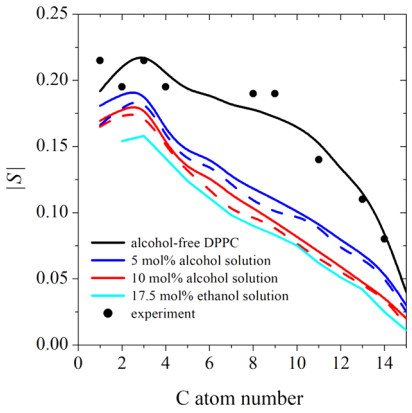

Figure 10. Deuterium order parameter for C−H bonds along hydrocarbon chains of lipid. The largest C atom number corresponds to the end C atom of the acyl chain. The markers indicate experimental data by Seelig and Seelig[60] for the alcohol-free DPPC at 323 K. The full and dashed curves indicate order parameters for ethanol- and *n*-propanol-dissolved bilayers, respectively. Mole fractions of ethanol (*n*-propanol) in ≈5 mol % and ≈10 mol % solutions are 0.520 (0.530) and 0.104(0.103), respectively.

that our calculated deuterium order parameter for the alcohol-free DPPC sample at 323 K is in close agreement with experimental data.[60] Both ethanol and *n*-propanol disorder the hydrocarbon chains: |S| decreases for all positions, approaching complete randomness in the center of the bilayer. In other words, lateral membrane expansion, due to the addition of alcohol, gives rise to orientational disordering of lipid chains. Obviously, the dissolved alcohol in the membrane alters the membrane function by its influence on the lipid order.

Further examination of alcohol effects on the lipid chains of the bilayer is done by comparing the density profiles for lipid chains of each leaflet in the absence and presence of alcohol. The results in Figure 11 first show that in the presence of alcohol, the lipid density is reduced due to dilution by alcohol molecules. Second, the distance between the two peaks corresponding to the head groups of the two opposite leaflets decreases, as already seen in Figure 2. On the other hand, the lipid density at the bilayer center increases. This is due to the interdigitation of lipid tails of each leaflet with the opposite layer,[61] which increases with alcohol concentration. The magnitude of interdigitation and decrease in the head-group density peak depends on the alcohol concentration; both effects are stronger at higher alcohol concentrations. Moreover, the effects are more pronounced for *n*-propanol than for ethanol. These observations indicate that concomitant with increasing the surface area of the bilayer and decreasing its thickness, alcohol introduces disorder in the bilayer. Finally, we note that also the lipid density profiles show the decrease of membrane thickness with the alcohol content. We have also

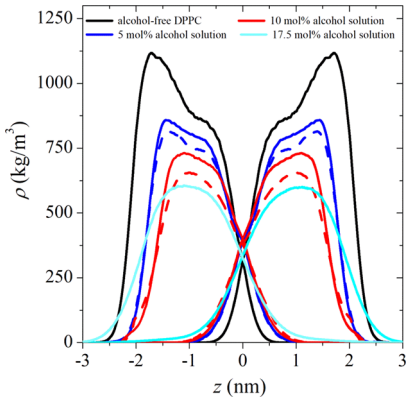

Figure 11. Density profiles for lipid chains of two opposite leaflets at 323 K. The full and dashed curves indicate profiles in ethanol- and *n*-propanol-dissolved bilayers, respectively. Mole fractions of ethanol (*n*-propanol) in ≈5 mol % and ≈10 mol % solutions are 0.520 (0.530) and 0.104(0.103), respectively.

plotted in Figure S2 the density profiles for lipid chains of each leaflet in the absence and presence of ethanol at 298 K. Expectedly, no noticeable effect of alcohol on the lipid phase, such as interdigitation of the lipid tails, is observed in the gel phase of DPPC.

SUMMARY AND CONCLUSIONS

We have performed GCE and metadynamics simulations to examine the role of alcohol-induced failure of the viral membrane as the deactivation mechanism of SARS-CoV-2. Our simulations propose that the highest alcohol concentration in the aqueous disinfectant solution at which the SARS-CoV-2 exterior membrane remains stable is 15 mol %. It is worth mentioning that the composition of the SARS-CoV-2 membrane is not known. Coronavirus membranes have a complex structure, holding a variety of proteins (required for their biological function) and presumably different phospholipids.[6] Owing to the structural complexity of the viral membranes, we have concentrated our simulation on a model membrane, pure DPPC, which is known as a useful model membrane for many practical purposes. We have done two sets of atomistic MD simulations; one at 323 K (above the gel-to-liquid crystalline phase transition temperature of DPPC, 315 K)[20] and another at 298 K (where DPPC exists in the gel phase) for a number of systems in which the concentration of ethanol varied systematically from 0 to 17.5 mol % (0 to 35.2 wt %) and that of *n*-propanol varied from 0 to 15.0 mol % (0 to 37.0 wt %) in the aqueous phase surrounding the membrane.

Our findings indicate that the solubility of alcohol in the membrane strongly depends on temperature, or more specifically, on the phase of the membrane. While alcohol does not have a considerable solubility and hence weakening effects on the gel phase of the membrane, a minimum alcohol concentration of 15 mol % is enough to disintegrate the membrane in its liquid crystalline phase. The membrane changes its structure, when exposed to disinfectant solutions. Both ethanol and *n*-propanol mainly dissolve in the hydrophilic−hydrophobic interphase of the membrane, i.e., alcohol solubility in the membrane is driven by both the interactions between the OH group of alcohol and the polar head groups of the membrane and the dissolution of the hydrophobic tail of alcohol among the hydrocarbon chains of the bilayer. Uptake of alcohol swells the membrane laterally but shrinks its

https://dx.doi.org/10.1021/acs.jpcb.0c08296
J. Phys. Chem. B 2020, 124, 10374−10385

thickness. At the same time, the orientational order of lipid tails decreases significantly. The shrinking of the membrane thickness shortens the gap that all penetrants need to cross from outside the virus into its core. Such an alcohol-induced weakening of the membrane has important consequences for the functioning of the membrane and, hence, the inactivation of the virus.

The lateral swelling of the membrane should lead to crumpling, lower bending stiffness, and ultimately higher propensity for perforation. As the membrane is responsible for mechanically anchoring the spike proteins, used by the virus for fusion to the host cell membranes, alcohol-induced softening of the membrane facilitates the loss of infectious proteins (inactivation of the virus infectivity prior to the membrane rupture).

Already aqueous solutions of 5 and 10 mol % alcohol have significant weakening effects on the membrane. The effects of *n*-propanol are always stronger than those of ethanol. The free-energy barrier to permeation by all permeants is significantly lowered by alcohol uptake. At a disinfectant concentration of 10 mol %, it becomes insignificant enough to allow almost free passage of the disinfectant to the inside of the virus to cause damage there. It should be noted that the disinfectant causes also the barrier for water permeation to drop. At alcohol concentrations in the disinfectant solution above 15 mol %, we reliably observe disintegration of the membrane.

Because of the tight packing of lipid molecules, the DPPC bilayer in its gel phase is less permeable to alcohol than that in the liquid crystalline phase. Although the same trend of alcohol weakening effects on the liquid crystalline phase of membrane is observed in the gel phase as well, the effect is less pronounced. However, this is mainly due to the fact that by reducing the temperature from 323 K to 298, the DPPC undergoes a phase transition (from liquid crystalline to gel). It is worth mentioning that although the structure of the lipid membrane of SARS-CoV-2 is not known, there is experimental evidence indicating structural similarities between SARS-CoV and HIV.[8] Experimental observations indicate that SARS and HIV peptides permeabilize the phospholipid membranes and reduce their gel-to-liquid crystalline phase transition temperatures.[10,17] Also, mixtures of PMPC, PPPC, and POPC (as the constituents of lung surfactants) with DPPC reduce the gel-to-liquid crystalline phase transition temperature of DPPC.[18,19] These observations imply that the fluid (liquid crystalline) phase of the bilayer is the most physically relevant phase to the inactivation of SARS-CoV-2 infectivity by alcohol. Therefore, we speculate that the effect of alcohol on weakening the liquid crystalline phase of DPPC (323 K), discussed in this work, is relevant to alcohol-induced failure of the viral membrane as the deactivation mechanism of SARS-CoV-2.

■ ASSOCIATED CONTENT

Supporting Information

The Supporting Information is available free of charge at https://pubs.acs.org/doi/10.1021/acs.jpcb.0c08296.

Ethanol penetration into the lipid bilayer and effect of ethanol on the structure of the lipid bilayer at 298 K (PDF)

■ AUTHOR INFORMATION

Corresponding Author

Hossein Eslami − *Eduard-Zintl-Institut für Anorganische und Physikalische Chemie, Technische Universität Darmstadt, Darmstadt 64287, Germany; Department of Chemistry, College of Sciences, Persian Gulf University, Boushehr 75168, Iran;* orcid.org/0000-0002-1990-0469; Email: h.eslami@theo.chemie.tu-darmstadt.de

Authors

Shubhadip Das − *Eduard-Zintl-Institut für Anorganische und Physikalische Chemie, Technische Universität Darmstadt, Darmstadt 64287, Germany*

Tianhang Zhou − *Eduard-Zintl-Institut für Anorganische und Physikalische Chemie, Technische Universität Darmstadt, Darmstadt 64287, Germany*

Florian Müller-Plathe − *Eduard-Zintl-Institut für Anorganische und Physikalische Chemie, Technische Universität Darmstadt, Darmstadt 64287, Germany;* orcid.org/0000-0002-9111-7786

Complete contact information is available at: https://pubs.acs.org/10.1021/acs.jpcb.0c08296

Notes

The authors declare no competing financial interest.

■ ACKNOWLEDGMENTS

We gratefully acknowledge the support of this work by the Deutsche Forschungsgemeinschaft (DFG), project MU1412/25-2, as well as through the SFB-TRR146 "Multiscale Simulation Methods for Soft Matter", project A8. H.E. also acknowledges the research department of Persian Gulf University for offering him the leave of absence.

■ REFERENCES

(1) Kampf, G.; Todt, D.; Pfaender, S.; Steinmann, E. Persistence of Coronaviruses on Inanimate Surfaces and Their Inactivation with Biocidal Agents. *J. Hosp. Infect.* **2020**, *104*, 246−251.

(2) Ly, H. V.; Longo, M. L. The Influence of Short-Chain Alcohols on Interfacial Tension, Mechanical Properties, Area/Molecule, and Permeability of Fluid Lipid Bilayers. *Biophys. J.* **2004**, *87*, 1013−1033.

(3) Wang, Y.; Dea, P. Interaction of 1-Propanol and 2-Propanol with Dipalmitoylphosphatidylcholine, Bilayer: A Calorimetric Study. *J. Chem. Eng. Data* **2009**, *54*, 1447−1451.

(4) Manca, M. L.; Castangia, I.; Matricardi, P.; Lampis, S.; Fernàndez-Busquets, X.; Fadda, A. M.; Manconi, M. Molecular Arrangements and Interconnected Bilayer Formation Induced by Alcohol or Polyalcohol in Phospholipid Vesicles. *Colloids Surf., B* **2014**, *117*, 360−367.

(5) Zhang, M.; Peyear, T.; Patmanidis, I.; Greathouse, D. V.; Marrink, S. J.; Andersen, O. S.; Ingólfsson, H. I. Fluorinated Alcohols' Effects on Lipid Bilayer Properties. *Biophys. J.* **2018**, *115*, 679−689.

(6) Fiani, B.; Covarrubias, C.; Desai, A.; Sekhon, M.; Jarrah, R. A Contemporary Review of Neurological Sequelae of Covid-19. *Front. Neurol.* **2020**, *11*, 1−9.

(7) Schoeman, D.; Fielding, B. C. Coronavirus Envelope Protein: Current Knowledge. *Virol. J.* **2019**, *16*, 69.

(8) Bafna, K.; Krug, R. M.; Montelione, G.. Structural Similarity of SARS-CoV2 Mpro and HCV NS3/4A Proteases Suggests New Approaches for Identifying Existing Drugs Useful as COVID-19 Therapeutics. ChemRxiv. 2020.

(9) Kupferschmidt, K.; Cohen, J. Race to Find COVID-19 Treatments Accelerates. *Science* **2020**, *367*, 1412−1413.

(10) Khattari, Z.; Brotons, G.; Akkawi, M.; Arbely, E.; Arkin, I. T.; Salditt, T. SARS Coronavirus E Protein in Phospholipid Bilayers: An X-Ray Study. *Biophys. J.* **2006**, *90*, 2038−2050.
(11) Neuman, B. W.; Kiss, G.; Kunding, A. H.; Bhella, D.; Baksh, M. F.; Connelly, S.; Droese, B.; Klaus, J. P.; Shinji Makino, S.; Sawicki, S. G.; Siddell, S. G.; Stamou, D. G.; Wilson, I. A.; Kuhn, P.; Buchmeier, M. J. A Structural Analysis of M Protein in Coronavirus Assembly and Morphology. *J. Struct. Biol.* **2011**, *174*, 11−22.
(12) Verdiá-Báguena, C.; Nieto-Torres, J. L.; Alcaraz, A.; DeDiego, M. L.; Torres, J.; Aguilella, V. M.; Enjuanes, L. Coronavirus E Protein Forms Ion Channels with Functionally and Structurally-Involved Membrane Lipids. *Virology* **2012**, *432*, 485−494.
(13) Bar-On, Y. M.; Flamholz, A.; Phillips, R.; Milo, R. SARS-CoV-2 (COVID-19) by the Numbers. *eLife* **2020**, *9*, No. e57309.
(14) Fung, T. S.; Liu, D. X. Human Coronavirus: Host-Pathogen Interaction. *Annu. Rev. Microbiol.* **2019**, *73*, 529−557.
(15) Stertz, S.; Reichelt, M.; Spiegel, M.; KuriLuis, T.; Martínez-Sobrido, L.; García-Sastre, A.; Weber, F.; Kochs, G. The Intracellular Sites of Early Replication and Budding of SARS-Coronavirus. *Virology* **2007**, *361*, 304−315.
(16) Holm, B. A.; Wang, Z.; Egan, E. A.; Notter, R. H. Content of in Lung Surfactant: Ramifications for Surface Activity. *Pediatr. Res.* **1996**, *39*, 805−811.
(17) Guillén, J.; Perez-Berna, A. J.; Moreno, M. R.; Villalaín, J. A Second SARS-CoV S2 Glycoprotein Internal Membrane-Active Peptide. Biophysical Characterization and Membrane Interaction. *Biochemistry* **2008**, *47*, 8214−8224.
(18) Keough, K. M. W.; Davis, P. J. Gel to Liquid-Crystalline Phase Transition in Water Dispersions of Saturated Mixed-acid Phosphatidylcholines. *Biochemistry* **2002**, *18*, 1453−1459.
(19) Svetlovics, J. A.; Wheaten, S. A.; Almeida, P. F. Phase Separation and Fluctuations in Mixtures of a Saturated and an Unsaturated Phospholipid. *Biophys. J.* **2012**, *102*, 2526−2535.
(20) Wiedmann, T.; Salmon, A.; Wong, V. Phase Behavior of Mixtures of DPPC and POPC. *Biochimica. Bipophysica. Acta.* **1993**, *1167*, 114−120.
(21) Chin, A. W. H.; Chu, J. T. S.; Perera, M. R. A.; Hui, K. P. Y.; Yen, H.-L.; Chan, M. C. W.; Peiris, M.; Poon, L. L. M. Stability of SARS-CoV-2 in Different Environmental Conditions. *Lancet Microbe.* **2020**, *1*, No. e10.
(22) Marrink, S. J.; Berendsen, H. J. C. Simulation of Water Transport through Lipid Membrane. *J. Phys. Chem.* **1994**, *98*, 4155−4168.
(23) Bemporad, D.; Luttmann, C.; Essex, J. W. Computer Simulation of Small Molecule Permeation across a Lipid Bilayer: Dependence on Bilayer Properties and Solute Volume, Size, and Cross-Sectional Area. *Biophys. J.* **2004**, *87*, 1−13.
(24) Benett, W. F. D.; Shea, J.-E.; Tieleman, D. P. Phospholipid Chain Interactions with Cholesterol Dtive Domain Formation in Lipid Membranes. *Biophys. J.* **2018**, *114*, 2595−2605.
(25) Lee, C. T.; Comer, J.; Herndon, C.; Leung, N.; Pavlova, A.; Swift, R. V.; Tung, C.; Rowley, C. N.; Amaro, R. E.; Chipot, C.; Wang, Y.; Gumbart, J. C. Simulation-Based Approaches for Determining Membrane Permeability of Small Compounds. *J. Chem. Inf. Model.* **2016**, *56*, 721−733.
(26) Melo, M. N.; Arnarez, C.; Sikkema, H.; Kumar, N.; Walko, M.; Berendsen, H. J. C.; Kocer, A.; Marrink, S. J.; Ingólfsson, H. I. High-Throughput Simulations Reveal Membrane-Mediated Effects of Alcohols on MscL Gating. *J. Am. Chem. Soc.* **2017**, *139*, 2664−2671.
(27) Müller, T. J.; Müller-Plathe, F. A Comparison of Sulfur Mustard and Heptane Penetrating a Dipalmitoylphosphatidylcholine Bilayer Membrane. *J. Hazard. Mater.* **2009**, *168*, 13−24.
(28) Venable, R. M.; Krämer, A.; Pastor, R. W. Molecular Dynamics Simulations of Membrane Permeability. *Chem. Rev.* **2019**, *119*, 5954−5997.
(29) Feller, S. E.; Brown, C. A.; Nizza, D. T.; Gawrisch, K. Nuclear Overhauser Enhancement Spectroscopy Cross-Relaxation Rates and Ethanol Distribution Across Membranes. *Biophys. J.* **2002**, *82*, 1396−1404.
(30) Gurtovenko, A. A.; Anwar, J. Interaction of Ethanol with Biological Membranes: The Formation of Non-bilayer Structures within the Membrane Interior and their Significance. *J. Phys. Chem. B* **2009**, *113*, 1983−1992.
(31) Kumari, P.; Kumari, M.; Kashyap, H. K. Counter-effects of Ethanol and Cholesterol on the Heterogeneous PSM−POPC Lipid Membrane: A Molecular Dynamics Simulation Study. *J. Phys. Chem. B* **2019**, *123*, 9616−9628.
(32) Lane, M. E. Skin Penetration Enhancers. *Int. J. Pharm.* **2013**, *447*, 12−21.
(33) Nagel, J. F.; Wiener, M. C. Structure of Fully Hydrated Bilayer Dispersions. *Biochim. Biophys. Acta* **1988**, *942*, 1−10.
(34) Klauda, J. B.; Venable, R. M.; Freites, J. A.; O'Connor, J. W.; Tobias, D. J.; Mondragon-Ramirez, C.; Vorobyov, I.; MacKerell, A. D., Jr.; Pastor, R. W. Update of the CHARMM All-atom Additive Force Field for Lipids: Validation on Six Lipid Types. *J. Phys. Chem. B* **2010**, *114*, 7830−7843.
(35) Müller-Plathe, F. YASP: A Molecular Simulation Package. *Comput. Phys. Commun.* **1993**, *78*, 77−94.
(36) Berendsen, H. J. C.; Postma, J. P. M.; van Gunsteren, W. F.; DiNola, A.; Haak, J. R. Molecular Dynamics with Coupling to an External Bath. *J. Chem. Phys.* **1984**, *81*, 3684−3690.
(37) Frenkel, D.; Smit, B. *Understanding Molecular Simulations*; Elsevier: San Diego, 2002.
(38) Hu, Y.; Ou, S.; Patel, S. Free Energetics of Arginine Permeation into Model DMPC Lipid Bilayers: Coupling of Effective Counterion Concentration and Lateral Bilayer Dimensions. *J. Phys. Chem. B* **2013**, *117*, 11641−11653.
(39) Awasthi, N.; Hub, J. S. Simulations of Pore Formation in Lipid Membranes: Reaction Coordinates, Convergence, Hysteresis, and Finite-Size Effects. *J. Chem. Theory Comput.* **2016**, *12*, 3261−3269.
(40) Eslami, H.; Müller-Plathe, F. Molecular Dynamics Simulation in the Grand Canonical Ensemble. *J. Comput. Chem.* **2007**, *28*, 1763−1773.
(41) Eslami, H.; Müller-Plathe, F. Molecular Dynamics Simulation of Sorption of Gases in Polystyrene. *Macromolecules* **2007**, *40*, 6413−−6421.
(42) Eslami, H.; Müller-Plathe, F. Water Permeability of Poly(ethylene terephthalate): A Grand Canonical Ensemble Molecular Dynamics Simulation Study. *J. Chem. Phys.* **2009**, *131*, 234904.
(43) Eslami, H.; Melis Kesik, M.; Karimi-Varzaneh, H. A.; Müller-Plathe, F. Sorption and Diffusion of Carbon Dioxide and Nitrogen in Poly(methyl methacrylate). *J. Chem. Phys.* **2013**, *139*, 124902.
(44) Rahbari, A.; Hens, R.; Moultos, O. A.; Dubbeldam, D.; Vlugt, T. J. H. Multiple Free Energy Calculations From Single State Point Continuous Fractional Component Monte Carlo Using Umbrella Sampling. *J. Chem. Theory Comput.* **2020**, *16*, 1757−1767.
(45) Patra, M.; Salonen, E.; Terama, E.; Vattulainen, I.; Faller, R.; Lee, B. W.; Holopainen, J.; Karttunen, M. Under the Influence of Alcohol: The Effect of Ethanol and Methanol on Lipid Bilayers. *Biophys. J.* **2006**, *90*, 1121−1135.
(46) Cordomi, A.; Edholm, O.; Perez, J. J. Effect of Ions on a Dipalmitoyl Phosphatidylcholine Bilayer. A Molecular Dynamics Simulation Study. *J. Phys. Chem. B* **2008**, *112*, 1397−1408.
(47) Bemporad, D.; Essex, J. W.; Luttmann, C. Permeation of Small Molecules through a Lipid Bilayer: A Computer Simulation Study. *J. Phys. Chem. B* **2004**, *108*, 4875−4884.
(48) Bassolino-Klimas, D.; Howard, E.; Alper, H. E.; Stouch, T. R. Mechanism of Solute Diffusion through Lipid Bilayer Membranes by Molecular Dynamics Simulation. *J. Am. Chem. Soc.* **1995**, *117*, 4118−4129.
(49) De Young, L. R.; Dill, K. A. Solute Partitioning into Lipid Bilayer Membranes. *Biochemistry* **2002**, *27*, 5281−5289.
(50) Rand, R. P.; Parsegian, V. A. Hydration Forces between Phospholipid Bilayers. *Biochim. Biophys. Acta* **1989**, *988*, 351−376.
(51) Schubert, T.; Schneck, E.; Tanaka, M. First Order Melting Transitions of Highly Ordered Dipalmitoylphosphatidylcholine Gel Phase Membranes in Molecular Dynamics Simulations with Atomistic Detail. *J. Chem. Phys.* **2011**, *135*, No. 055105.

https://dx.doi.org/10.1021/acs.jpcb.0c08296
J. Phys. Chem. B 2020, 124, 10374−10385

(52) Zhang, B. W.; Cui, D.; Matubayasi, N.; Levy, R. M. The Excess Chemical Potential of Water at the Interface with a Protein from End Point Simulations. *J. Phys. Chem. B.* **2018**, *122*, 4700−4707.
(53) Paliwal, A.; Asthagiri, D.; Pratt, L. R.; Ashbaugh, H. S.; Paulaitis, M. E. An Analysis of Molecular Packing and Chemical Association in Liquid Water Using Quasichemical Analysis. *J. Chem. Phys.* **2006**, *124*, 224502.
(54) Deng, Y.; Roux, B. Hydration of Amino Acid Side Chains: Nonpolar and Electrostatic Contributions Calculated from Staged Molecular Dynamics Free Energy Simulations with Explicit Water Molecules. *J. Phys. Chem. B* **2004**, *108*, 16567−16576.
(55) Zygmunt, W.; Potoff, J. J. The Effect of Florination on the Physical Properties and the Free Energies of Hydration of 1-alcohols. *Fluid Phase Equilib.* **2016**, *407*, 314−321.
(56) Kelly, C. P.; Cramer, C. J.; Truhlar, D. G. SM6: A Density Functional Theory Continuum Solvation Model for Calculating Aqueous Solvation Free Energies of Neutrals, Ions, and Solute-Water Clusters. *J. Chem. Theory Comput.* **2005**, *1*, 1133−1152.
(57) Laio, A.; Parrinello, M. Escaping Free Energy Minima. *Proc. Natl. Acad. Sci. U. S. A.* **2002**, *99*, 12562−12566.
(58) Eslami, H.; Khanjari, N.; Müller-Plathe, F. Self-Assembly Mechanisms of Triblock Janus Particles. *J. Chem. Theory Comput.* **2018**, *15*, 1345−1354.
(59) Khanjari, N.; Eslami, H.; Müller-Plathe, F. Adaptive-Numerical Bias Metadynamics. *J. Comput. Chem.* **2017**, *38*, 2721−2729.
(60) Seelig, A.; Seelig, J. The Dynamic Structure of Fatty Acyl Chains in a Phospholipid Bilayer Measured by Deuterium Magnetic Resonance. *Biochemistry* **2002**, *13*, 4839−4845.
(61) Dickey, A. N.; Yim, W.-S.; Faller, R. Using Ergosterol to Mitigate the Deleterious Effects of Ethanol on Bilayer Structure. *J. Phys. Chem. B* **2009**, *113*, 2388−2397.

https://dx.doi.org/10.1021/acs.jpcb.0c08296
J. Phys. Chem. B 2020, 124, 10374−10385